

# Learning Spatiotemporal Chaos Using Next-Generation Reservoir Computing

Wendson A. S. Barbosa<sup>1</sup> and Daniel J. Gauthier<sup>1,2</sup>

<sup>1</sup>*Department of Physics, The Ohio State University, 191 W. Woodruff Ave., Columbus, OH 43210, USA*

<sup>2</sup>*ResCon Technologies, LLC, PO Box 21229, Columbus, OH 43221, USA.*

(\*Electronic mail: [gauthier.51@osu.edu](mailto:gauthier.51@osu.edu).)

(\*Electronic mail: [desabarbosa.1@osu.edu](mailto:desabarbosa.1@osu.edu).)

Forecasting the behavior of high-dimensional dynamical systems using machine learning requires efficient methods to learn the underlying physical model. We demonstrate spatiotemporal chaos prediction using a machine learning architecture that, when combined with a next-generation reservoir computer, displays state-of-the-art performance with a training time  $10^3 - 10^4$  times faster and training data set  $\sim 10^2$  times smaller than other machine learning algorithms. We also take advantage of the translational symmetry of the model to further reduce the computational cost and training data, each by a factor of  $\sim 10$ .

**Modeling and predicting high-dimensional dynamical systems, such as spatiotemporal chaotic systems, continues to be a physics grand challenge and require efficient methods to leverage computational resources and efficiently process large amounts of data. In this work, we implement a highly efficient machine learning (ML) parallel scheme for spatiotemporal forecasting where each model unit predicts a single spatial location. This reduces the number of trainable parameters to the minimum number possible, thus speeding up the algorithm and reducing the data set size needed for training. Moreover, when combined with next-generation reservoir computers (NG-RCs), our approach presents state-of-the-art performance with a computational cost and training data dramatically reduced in comparison to other machine learning approaches. We also show that the computational cost and training data set size can be further reduced when the system display translational symmetry, which is commonly present in spatiotemporal systems with cyclic boundary conditions. Although many real systems do not have such symmetry, our results highlight the importance of symmetry addressing when it is present in the system.**

use ML algorithms, such as deep learning,<sup>6,14</sup> time embedding techniques<sup>15-17</sup> or sparse system identifiers,<sup>18</sup> to learn the underlying ordinary or partial differential equations, but this subsequently requires precise numerical methods for model integration. Another approach is to learn the system *flow*, which allows for one-step-ahead prediction using a coarser spatiotemporal grid, likely leading to faster prediction. The next-generation reservoir computer (NG-RC), for example, excels at this task,<sup>17</sup> and is mathematically equivalent to a traditional reservoir computer (RC) but has an optimal form.<sup>19</sup>

In typical ML approaches, the spatial variable is discretized at  $L$  points with step size  $\delta L$ , assumed one-dimensional for exposition simplicity, and time is discretized with step size  $\delta t$ . During supervised training, blocks of data with  $N_{in}$  spatial points and  $k$  time steps are fed into the artificial neural network (ANN) used to predict the behavior at  $N_{out}$  locations at one or more temporal steps. Often,  $N_{in} = N_{out} = L$  and  $k\delta t$  is longer than the correlation time,<sup>6,20</sup> which is problematic because it causes the model to focus on unrelated observations. Also, the ANN is large, which increases the number of trainable parameters and hence increases the required computer resources and training data set size. Recently, a parallel reservoir computing scheme<sup>21</sup> was introduced with  $N_{out} < N_{in} < L$  to reduce the computational cost.

Here, our primary contribution is to demonstrate a new algorithm for learning spatiotemporal systems. It makes predictions of the temporal dynamics of the system at a single spatial location based on data drawn from a small spatiotemporal neighborhood of the point. Prediction over all spatial points is realized using parallel machines. Quantitatively, we take  $N_{in} < L$  and  $N_{out} = 1$ , where  $N_{in}\delta L$  is less than or comparable to the spatial correlation length, and take  $k$  so that  $k\delta t$  is less than the correlation time. Hence, we use  $L$  parallel ANNs for one-step-ahead prediction. We apply our method to a heuristic atmospheric weather model using the NG-RC<sup>17</sup> as the core learning machine, which reduces the computational complexity and the data set size required for training while displaying state-of-the-art accuracy. Accounting for the translational symmetry of this model further reduces the training time and data. Figure 1 illustrates our scheme.

We highlight that addressing symmetries has proven to be

## I. INTRODUCTION

Many nonlinear systems display temporal dynamics that depend on spatial location, such as the heart,<sup>1</sup> optical devices,<sup>2</sup> and fluid flow.<sup>3</sup> These systems may display spatiotemporal chaos, which has finite spatiotemporal correlations, a loss of long-term predictability,<sup>4</sup> and the appearance of coherent structures.<sup>3</sup> Also, these systems often display multi-scale behavior, where information and energy flow across scales. Modelling spatiotemporal chaos is difficult for these reasons and continues to be a physics grand challenge.

One approach to this problem is to use machine learning, which may speed up prediction by learning only variables of interest, such as the macroscale behavior,<sup>5-7</sup> or improve the prediction accuracy by fusing model predictions and experimental observations.<sup>8-13</sup> Some researchers

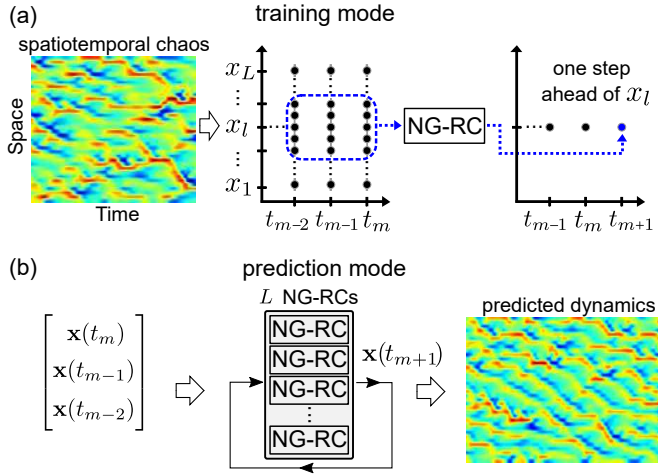


FIG. 1. Learning and predicting spatiotemporal chaos using our parallel scheme. (a) **Learning Mode:** The NG-RC is trained to predict the next time step  $t_{m+1}$  at the  $l^{\text{th}}$  spatial location using training data from the current  $t_m$  and previous steps  $t_{m-1}$  and  $t_{m-2}$  ( $k = 3$ ), and the  $N_{in} = 5$  neighbors. (b) **Prediction mode:** Autonomous operation of  $L$  parallel NG-RCs where the output feeds the input to predict the next step of all spatial locations  $\mathbf{x} = [x_1, x_2, \dots, x_L]$ .

important for improving other ML approaches.<sup>22–26</sup> Furthermore, ML algorithms can reveal hidden symmetries, such as translational invariance present in a simple 1D uniform motion or black hole dynamics,<sup>27</sup> even if their presence is not obvious.

The rest of the paper is organized as follows. In Sec. II, we formally describe the high-dimensional dynamical system used as the learning system to train our ML approach for spatiotemporal chaos prediction. In Sec. III, we describe our parallel scheme of ML models where each model unit predicts a single discretized spatial location represented by a system variable. In Sec. IV we introduce the theoretical background of the NG-RC, followed by brief descriptions of the training procedure and prediction mode. Section V is dedicated to the results. Here, we use our parallel scheme of NG-RCs to forecast high-dimensional chaos from the model equations introduced in Sec. II. We compare the cases where the parallel NG-RCs are trained independently to the case where a translational symmetry is taken into account to improve the performance. Finally, we apply our approach to a lower dimensional case of Lorenz96 model system and to an even lower dimensional case where fine-scale variables are not present. Lastly, we present a discussion comparing our results to other works and our conclusions in Sec. VI. We also include details on Ridge regression parameter optimization and computational complexity in the appendix.

## II. EXTENDED LORENZ96 MODEL

We demonstrate our approach using numerically generated data from a heuristic atmospheric weather model introduced by Lorenz<sup>4,28</sup> and extended by Thornes *et al.*<sup>29</sup> It has an unspecified macroscopic scalar variable  $x_l$  on a discrete grid (po-

sition  $l$ ) representing the observations around a latitude circle. To represent some convective-scale quantity across spatiotemporal scales, this variable is driven by a finer-scale variable  $y_{j,l}$ , which is coupled to the macroscopic variable as well as the finest scale variable  $z_{i,j,l}$  representing, for example, individual clouds in the atmosphere.

The model is described by a set of coupled differential equations given by

$$\begin{aligned} \dot{x}_l &= x_{l-1}(x_{l+1} - x_{l-2}) - x_l + F - \frac{hc}{b} S_{y_l}, \\ \dot{y}_{j,l} &= -cby_{j+1,l}(y_{j+2,l} - y_{j-1,l}) - cy_{j,l} + \frac{hc}{b} x_l - \frac{he}{d} S_{z_{j,l}}, \\ \dot{z}_{i,j,l} &= edz_{i-1,j,l}(z_{i+1,j,l} - z_{i-2,j,l}) - ge z_{i,j,l} + \frac{he}{d} y_{j,l}, \end{aligned} \quad (1)$$

where the indices  $l = 1, \dots, L$ ,  $j = 1, \dots, J$  and  $i = 1, \dots, I$  are  $\text{mod}(l, L)$ ,  $\text{mod}(j, J)$ , and  $\text{mod}(i, I)$ , respectively, to represent cyclic boundary conditions. The terms  $S_{y_l} = \sum_{j=1}^J y_{j,l}$  and  $S_{z_{j,l}} = \sum_{i=1}^I z_{i,j,l}$  represent the couplings between the different spatiotemporal scales.

Here,  $F = 20$  is a spatially homogeneous, large-scale forcing term,  $h = 1$  is the coupling strength between the different spatial scales and the parameters  $b = c = d = e = g = 10$  set the magnitude and time scale of the fast variables. With these parameters, there is a factor of 100 difference in spatiotemporal scales from the finest ( $z$ ) to the coarsest ( $x$ ) scale. For future reference, we specify time in model time units (MTU), where 1 MTU corresponds approximately to 5 atmospheric days.<sup>4</sup> We take  $L = 36$  to set the number of coherent structures appropriate for the Earth's weather and  $J = 10$ .<sup>4</sup> For the fastest variable, we take  $I = J$  following previous studies.<sup>6,7</sup> There are  $L * J = 360$  fine-scale and  $L * J * I = 3,600$  finest-scale variables and hence there are  $L[1 + J(1 + I)] = 3,996$  total variables.

We focus on learning and predicting only the slow macroscopic variables  $x_l$  without observing the finer-scale dynamics.<sup>6,7,30</sup> Because of the fast time scale of  $y_{l,j}$  and  $z_{i,j,l}$  in comparison to  $x_l$ ,  $S_{y_l}$  acts as a noise-like term in driving  $x_l$ . It is known that many ML algorithms, including an NG-RC,<sup>17</sup> can learn in the presence of large noise and hence we expect that we can make accurate predictions as demonstrated below.

## III. THE PARALLEL ML SCHEME

Our goal is to learn the one-step-ahead dynamics at a single location  $x_l$  based on using  $N_{in} = (2N_{nn} + 1)$  spatial points and  $k$  temporal points, illustrated by the dashed boundary shown in the middle panel of Fig. 1a, shown for  $N_{nn} = 2$ ,  $N_{in} = 5$ , and  $k = 3$ , values we use in the results section below. We seek an ML model that predicts  $x_l$  at time step  $t_{m+1}$  based on this input data. Thus, there are  $L$  independent ML models to predict the dynamics at all spatiotemporal points. Our scheme can work with a variety of ML algorithms but we use an NG-RC because of its proven ability to make accurate predictions with limited data and low computational resources.<sup>17</sup>

#### IV. THE NG-RC

We operate the NG-RC in two modes shown in Fig. 1: training and forecasting. In both cases, we create a feature vector

$$\mathcal{O}_{l,total}(t_m) = c \oplus \mathcal{O}_{l,lin} \oplus \mathcal{O}_{l,nonlin} \quad (2)$$

composed of linear and nonlinear parts, respectively, where  $c$  is a constant and  $\oplus$  is the concatenation operator. The linear part is formed by the current and previous  $k-1$  values of the variable  $x_l$  and its  $N_{nn}$  nearest neighbors of each side of this location. Hence, the dimension of  $\mathcal{O}_{l,nonlin}$  is  $d_{lin} = kN_{nn} = 15$  for our choice of parameters.

We take the nonlinear part to be the unique second-order monomials of  $\mathcal{O}_{l,lin}$ , which is appropriate for this problem because Eqs. 1 contains only quadratic nonlinear terms. For the unique quadratic monomials, the dimension of  $\mathcal{O}_{l,nonlin}$  is  $d_{nonlin} = d_{lin}(d_{lin} + 1)/2 = 120$  so that the total feature vector  $\mathcal{O}_{l,total}$  has  $d_{total} = 1 + d_{lin} + d_{nonlin} = 136$  components, which is also equal to the number of trainable parameters for each NG-RC. Minimizing  $d_{total}$  is one important metric for reducing the computational resources during training. As an aside, we mention that other nonlinear functions can be used in the NG-RC, such as higher-order polynomials or radial basis functions, but are not needed here.

During training, data from the solution to Eqs. 1 with  $N_{in}$  spatial points and  $M$  temporal points ( $t_{train} = M\delta t$  training time) is fed into each NG-RC ( $L$  total) in an open-loop manner as illustrated in Fig. 1a. Here, the goal is to have the one-step-ahead prediction  $\bar{x}_l(t_{m+1})$  of the NG-RC equal to the model prediction  $x_l(t_{m+1})$ , where  $t_{m+1} = t_m + \delta t$ . That is, we seek a solution to

$$\bar{x}_l(t_{m+1}) = \mathbf{W}_l \mathcal{O}_{l,total}(t_m) \quad (3)$$

that minimizes  $\|\bar{x}_l - x_l\|^2 + \alpha \|\mathbf{W}_l\|^2$  over all  $M$  temporal points. Here,  $\mathbf{W}_l$  is found using regularized regression with regularization parameter  $\alpha$  (see appendix A for  $\alpha$  optimization). For our parameters,  $\mathbf{W}_l$  is a  $(1 \times d_{total}) = (1 \times 136)$  matrix. For future reference, the computational complexity of training a single NG-RC scales as  $Md_{total}^2$  and hence as  $LMd_{total}^2$  for all  $L$  NG-RCs.

After finding  $\mathbf{W}_l$ , we switch to prediction mode, where the training data is no longer input. The output of each NG-RC is sent to the input in a closed-loop manner and used to create  $\mathcal{O}_{l,total}(t)$  for each NG-RC as shown in Fig. 1b. The parallel NG-RCs now form an autonomous spatiotemporal dynamical system. Here, the ‘warm up’ of the NG-RC requires  $k$  previous time steps as the initial conditions, which is often available if we immediately switching to the forecasting mode from the training mode.

#### V. RESULTS

##### A. $L$ independent NG-RCs

To test the accuracy and speed of our new algorithm, we generate spatiotemporal data by integrating Eqs. 1 using a

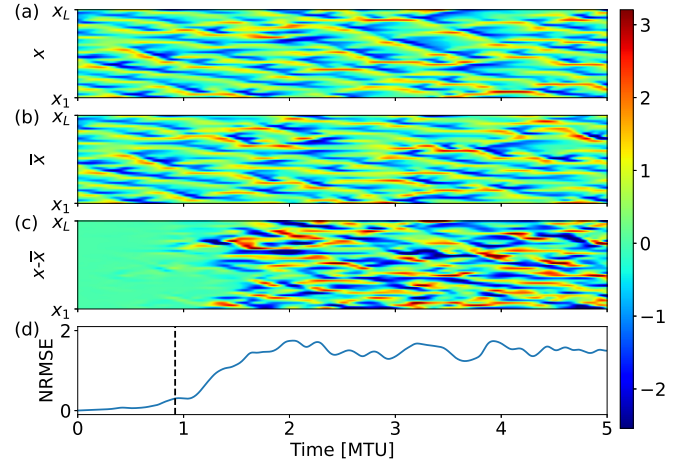


FIG. 2. Spatiotemporal dynamics prediction with parallel NG-RCs using  $L$  independent  $\mathbf{W}_l$ 's. (a) Actual and (b) predicted dynamics for the extended Lorenz96 model. (c) Difference and (d) NRMSE between actual and predicted dynamics. The vertical dashed line indicates the prediction horizon. Parameters:  $k = 3$ ,  $N_{nn} = 2$  and  $\alpha = 10^{-2}$ .

fourth order Runge-Kutta method with fixed step size of 0.001 MTU, where we save data at steps of  $\delta t = 0.01$  MTU. We use initial conditions  $x_1 = F + 0.01$ ,  $x_{l \neq 1} = F$  and  $y_{j,l} = z_{i,j,l} = 0$ , integrate for 10 MTU to dissipate transients and discard this data. We integrate for an additional 2,100 MTU to generate the data from which we select an interval  $t_{train}$  ( $M = t_{train}/\delta t$ ) to use as training data set. After integration, we normalize the data to have zero mean and unit standard deviation. After training, we select  $k$  consecutive time steps to warm up the NGRCs for the prediction mode and select the following 5 MTU time interval to generate the ground-truth test data (data never seen by the NG-RCs during training), an example of which is shown in Fig. 2a.

Figure 2b shows the NG-RC-predicted spatiotemporal dynamics of the extended Lorenz96 model using  $t_{train} = 10$  MTU ( $M = 1,000$ ). Here, we train  $L = 36$  NG-RCs, each with  $d_{total} = 136$ . The difference between ground-truth and prediction are initially small (Fig. 2c), but eventually diverge because the chaotic nature of the system will amplify small difference between the two. Even though long-term prediction is lost, the predicted behavior has coherent structures that are visually similar to the extended Lorenz96 model.

To quantify the prediction quality, we determine the normalized root-mean-square error over all spatial locations given by

$$\text{NRMSE}(t) = \sqrt{\frac{1}{L} \sum_{l=1}^L (x_l(t) - \bar{x}_l(t))^2}. \quad (4)$$

The right-hand side of Eq. 4 is already normalized in our case because  $x_l$  has unit standard deviation. As shown in Fig. 2d, the NRMSE increases from nearly zero, eventually reaching a saturated value. We define a prediction horizon as the time where  $\text{NRMSE}=0.3$  (vertical dashed line), which is equal to 0.92 for the single prediction realization shown in Fig. 2.

When averaged over 100 predictions for different initial conditions, the prediction horizon is equal to  $0.66 \pm 0.15$  MTU, or approximately  $3.2 \pm 0.7$  atmospheric days for the extended Lorenz96 model. We comment on the accuracy of our prediction in the discussion section below.

### B. Using translational symmetry

We further decrease the training data set size by taking into account the translational invariance of the extended Lorenz96 model given in Eq. 1, which arises from the cyclic boundary conditions and the spatially-independent model parameters. Because of this symmetry,  $\mathbf{W}_l$  should be independent of  $l$  in the asymptotic limit  $t_{train} \rightarrow \infty$ . To quantify the independence for the finite  $t_{train}$  used here, we measure the similarity of the  $\mathbf{W}_l$ 's by defining a correlation coefficient

$$C = \frac{1}{L(L-1)} \sum_l \sum_{l' \neq l} \frac{\mathbf{W}_l^T \cdot \mathbf{W}_{l'}^T}{\|\mathbf{W}_l\|^2}, \quad (5)$$

where  $T$  is the transpose operation,  $\cdot$  is the dot product operation, and  $C = 1$  ( $C = 0$ ) indicates (un)correlated matrices. For the case presented in Fig. 2, we find that it is equal to 0.96, indicating that the NG-RC does a reasonable job of discovering this symmetry even with short  $t_{train}$ .

We force translational symmetry by training a single  $\mathbf{W}$  and use it for all spatial locations  $l$ . Operationally, we concatenate all  $\mathcal{O}_{l,total}$  to create a data structure that has dimension  $L M d_{total}$  and hence the training computational complexity scales as  $L M d_{total}^2$ , the same as in the previous scheme. This procedure relies on the fact that each spatial location has identical behavior - in a statistical sense - and hence all the data is produced by the same underlying dynamical flow. Effectively, it increases the training time to  $L t_{train}$  for an observation time  $t_{train}$  of the spatiotemporal dynamics. A similar approach has been used recently when using a traditional RC for forecasting spatiotemporal dynamics.<sup>31</sup>

Accounting for the translational symmetry somewhat improves the prediction horizon for the same training data size, *i.e.*, the same value of  $M$ , as seen in Fig. 3, which displays a prediction horizon of 1.04 for the same initial condition used in Fig. 2. The mean prediction horizon for 100 different initial conditions increases by  $\sim 29\%$  to  $0.85 \pm 0.17$  MTU.

### C. Prediction accuracy comparison

As seen in Fig. 4, the prediction horizon for  $L$  independent NG-RCs is near zero (poor prediction ability), begins to improve for  $t_{train} \gtrsim 2$ , and saturates above  $t_{train} \gtrsim 20$ . On the other hand, we obtain reasonable performance when respecting the translational symmetry for the smallest training time shown in the plot, and we obtain nearly the same prediction performance as the other approach for  $t_{train} \gtrsim 1$ . Thus, we see that we can reduce the observation time and computational cost by  $\sim 1/L$ , which is expected because the effective training time is  $L$  times longer.

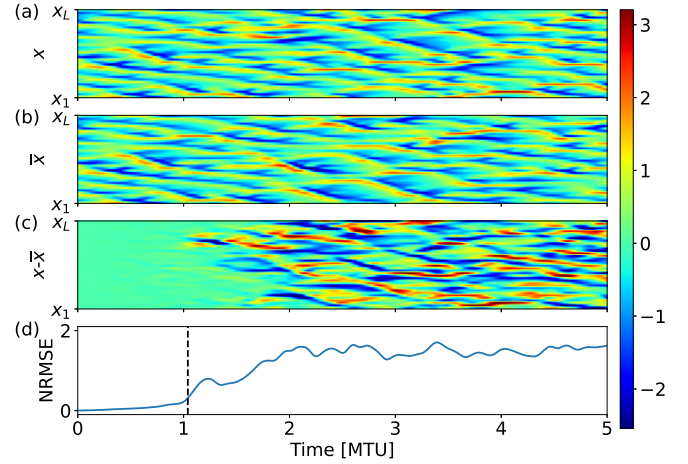


FIG. 3. Spatiotemporal dynamics prediction with parallel NG-RCs using a single  $\mathbf{W}$  that respects translational symmetry. (a) Actual and (b) predicted dynamics for the extended Lorenz96 model. (c) Difference and (d) NRMSE between actual and predicted dynamics. The vertical dashed line indicates the prediction horizon. Parameters:  $k = 3$ ,  $N_{mn} = 2$  and  $\alpha = 10^{-2}$ .

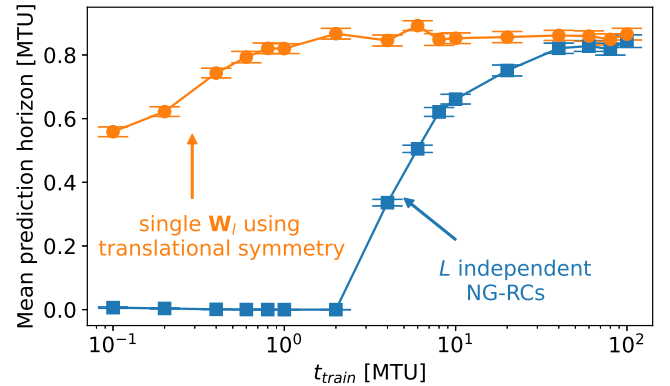


FIG. 4. Scaling of the mean prediction horizon with training time for the parallel NG-RCs using  $L$  independent  $\mathbf{W}_l$ 's (blue square) and using a single  $\mathbf{W}_l$  that respects translational symmetry (orange circles). Symbols represent the mean prediction horizon for 10 different training sets. For each training set we make predictions for 10 different initial conditions, total 100 predictions per point in the plot. Error bars represent the standard deviation of the mean over the 100 predictions. Parameters:  $k = 3$ ,  $N_{mn} = 2$  and  $\alpha$  is optimized for each  $t_{train}$  (see appendix A).

### D. Lower dimensional cases for the Lorenz 96 model

Here, we apply our model to lower dimensional cases of the extended Lorenz96 model. In section VI, we compare our results presented in the following to previous research that use such simplified models.

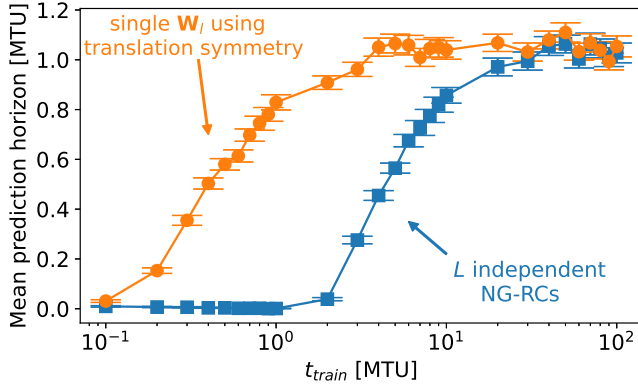


FIG. 5. Mean prediction horizon for Lorenz96 system with  $L = J = I = 8$  as function of  $t_{train}$  for the parallel NG-RCs using  $L$  independent  $\mathbf{W}_l$ 's (blue square) and using a single  $\mathbf{W}_l$  that respects translational symmetry (orange circles). Symbols represent the mean prediction horizon for 10 different training sets. For each training set we make predictions for 10 different initial conditions, totaling 100 predictions per point in the plot. The error bars represent the standard deviation of the mean over the 100 predictions. Parameters:  $k = 3$ ,  $N_{nn} = 2$  and  $\alpha$  is optimized for each  $t_{train}$ .

### 1. Parallel NG-RC model for $L = J = I = 8$

First, we apply our parallel NG-RC approach ( $N_{in} = 5, N_{out} = 1$ ) to the extended Lorenz96 system with  $L = J = I = 8$ . Figure 5 shows the mean prediction horizon as function of the training time  $t_{train}$  for our approach. When using  $L$  independent NG-RCs (blue squares), our model obtains a mean prediction horizon of  $1.05 \pm 0.38$  MTU with a training time  $t_{train} = 40$  MTU ( $M = 4,000$  training points). Here, each one of the  $L$  parallel NG-RCs are trained individually with  $M$  training points from the respective region. On the other hand, when using a single  $\mathbf{W}$  that respects the translation symmetry (orange circles), we obtain a similar result (with no statistical difference) for  $t_{train} = 4$  MTU, a training time reduced by a factor of  $\sim L$ . This reduction is expected because data from all  $L$  spatial locations are concatenated to form a single training data set in this method with an effective size is  $L$  times longer than  $t_{train} = 4$  MTU. Figure 6 shows typical predictions for both cases discussed above.

### 2. Parallel NG-RC model for the Lorenz96 model without fine-scale variables with $L = 40, J = I = 0$

Here, we use our approach to predict dynamics of a simpler Lorenz96 model that does not include the fine spatiotemporal variables  $y_{j,l}$  and  $z_{i,j,l}$  ( $J = I = 0$  - see Eq. 1). Here, we use  $L = 40$ . Figure 7 shows the mean prediction horizon as function of the training time  $t_{train}$ . When using  $L$  independently trained NG-RCs (blue squares), the performance begins to improve for  $t_{train} \gtrsim 2$  and saturates for  $t_{train} = 60$  where the mean prediction horizon is  $8.0 \pm 1.7 \Lambda$ . Here,  $\Lambda = 1/\lambda = 1/1.68$  MTU is the Lyapunov time for the Lorenz96 system with  $L = 40$  and  $F = 8$  (parameters used here).<sup>14</sup> On the other hand, when using a single  $\mathbf{W}$  that respects the translation symmetry

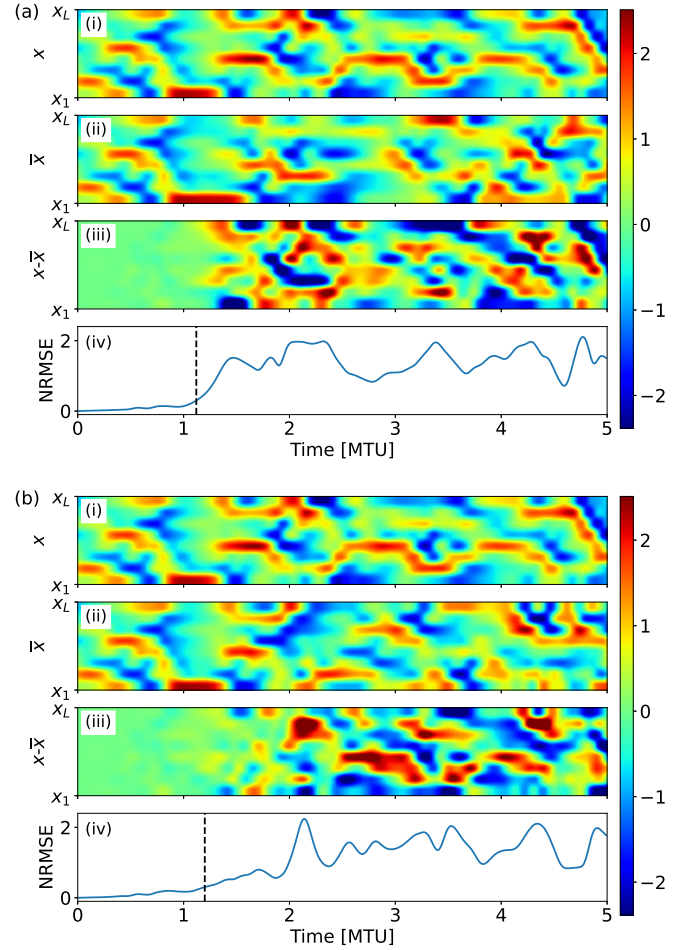


FIG. 6. Typical prediction for the extended Lorenz96 system with  $L = J = I = 8$  using our parallel NG-RC approach with  $N_{in} = 5$  and  $N_{out} = 1$ . (a) Using  $L$  independent  $\mathbf{W}_l$ 's with  $t_{train} = 40$  MTU and  $\alpha = 10^{-1}$ . (b) Using a single  $\mathbf{W}$  that respects translational symmetry with  $t_{train} = 4$  MTU and  $\alpha = 1.3 \times 10^{-1}$ . For both panels: (i) Actual and (ii) predicted dynamics, (iii) difference between actual and predicted dynamics, and (iv) NRMSE. The vertical dashed line indicates the prediction horizon. Parameters:  $k = 3$  and  $N_{nn} = 2$ .

(orange circles), our model obtains a mean prediction horizon of  $7.7 \pm 1.7 \Lambda$  using a training time of  $t_{train} = 1$  MTU. In other words, a similar prediction horizon (with no statistical difference) is obtained using a factor of 60 smaller training data set in comparison to the  $L$  independent NG-RCs case. Figure 8 shows typical predictions for both cases.

## VI. DISCUSSIONS AND CONCLUSIONS

We compare our results to previous research to demonstrate that our method is more accurate, or can be training with less data and computational cost, or both. Pyle *et al.*<sup>7</sup> use  $N_{in} = N_{out} = L$  and an algorithm similar to the NG-RC except that they only consider  $k = 1$  and use all monomials up to quartic order. They use  $L = 8$ , which is too small to serve as a model for the Earth's atmosphere. As presented in Sec.

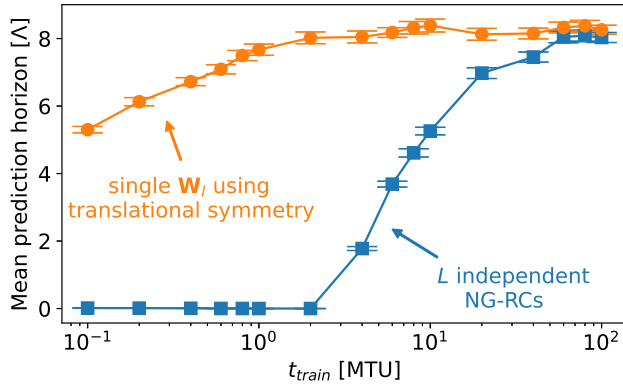


FIG. 7. Mean prediction horizon for Lorenz96 system with ( $L = 40$ ,  $J = I = 0$ ) as function of  $t_{train}$  for the parallel NG-RCs using  $L$  independent  $\mathbf{W}_l$ 's (blue square) and using a single  $\mathbf{W}_l$  that respects translational symmetry (orange circles). Symbols represent the mean prediction horizon for 10 different training sets. For each training set we make predictions for 10 different initial conditions, totaling 100 predictions per point in the plot. Error bars represent the standard deviation of the mean over the 100 predictions. Parameters:  $k = 3$ ,  $N_{nn} = 2$  and  $\alpha$  is optimized for each  $t_{train}$ .

**VD1**, we apply our approach for their parameters and find similar results with a training  $\sim 2 \times 10^3$  times faster using a factor of  $\sim 10^3$  less training data (See appendix B for computational complexity comparison).

Chattopadhyay *et al.*<sup>6</sup> also use  $N_{in} = N_{out} = L = 8$  and a traditional RC with  $d_{total} = 5,000$  nodes (equal to the size of their feature vector) and  $M = 500,000$  training steps, for which they obtain a similar prediction horizon to Pyle *et al.* Based on the computational complexity scaling (see appendix B), we find that our approach results in a factor of  $\sim 2 \times 10^5$  shorter computation training time and a factor of  $\sim 10^3$  smaller training data set when applying our approach to the same problem, as shown in Sec. **VD1**. Chattopadhyay *et al.* also implement a deep learning network, but this method demonstrates no accuracy improvement and requires more computation time.

Vlachas *et al.*<sup>14</sup> use a parallel RC scheme<sup>21</sup> to predict dynamics of a simpler Lorenz96 model with  $L = 40$  and  $J = I = 0$  and hence without fine-scale variables. They use 20 parallel RCs, each of size  $d_{total} = 3,000$  nodes,  $N_{in} = 10 > N_{out} = 2$ , and  $M = 100,000$ . As demonstrated in Sec. **VD2**, when applying our approach to this problem, we find a prediction horizon 2.4 times longer than their results using a training data set  $10^3$  times smaller and with a computational complexity  $\sim 2.4 \times 10^5$  times shorter.

Recently, Platt *et al.*<sup>32</sup> optimized the parallel RC architecture and obtained a mean prediction horizon twice as long as Vlachas *et al.* using  $N_{in} = 6 > N_{out} = 2$  with smaller RCs (each with  $d_{total} = 720$  nodes) and training data set ( $M = 40,000$ ). Our model obtains a slightly better performance in the mean prediction horizon with a computational complexity  $5.6 \times 10^3$  shorter using  $4 \times 10^2$  less training data than Platt.

To give an absolute scale for the computational cost for our approach, we produce the results for this paper using Python

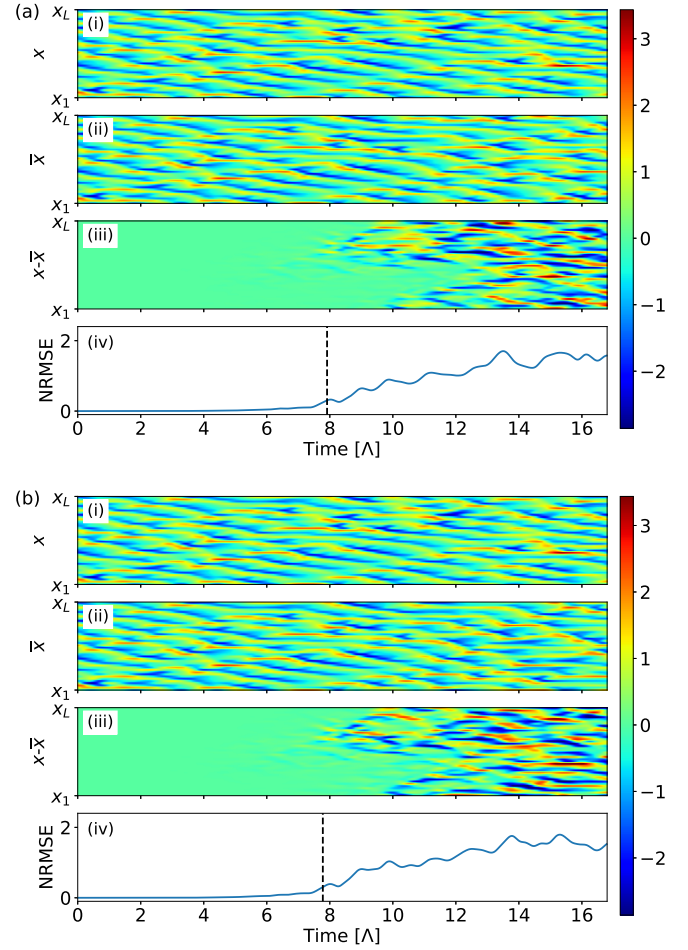


FIG. 8. Typical prediction for the extended Lorenz96 system with  $L = 40$ , and  $J = I = 0$  using our parallel NG-RC approach with  $N_{in} = 5$  and  $N_{out} = 1$ . (a) Using  $L$  independent  $\mathbf{W}_l$ 's with  $t_{train} = 60$  MTU and  $\alpha = 2 \times 10^{-5}$ . (b) Using a single  $\mathbf{W}$  that respects translational symmetry with  $t_{train} = 1$  MTU and  $\alpha = 1 \times 10^{-5}$ . For both panels: (i) Actual and (ii) predicted dynamics, (iii) difference between actual and predicted dynamics, and (iv) NRMSE. The vertical dashed line indicates the prediction horizon. Parameters:  $k = 3$  and  $N_{nn} = 2$

3.7.6, NumPy 1.19.15 and scikit-learn 0.24.2 on an x86-64 CPU running Windows 10. For the results presented in Figs. 2 and 3, the computation time for training all  $L = 36$  NG-RCs with  $M = 1,000$  data points is  $55 \pm 1$  ms while the runtime for predicting one time step is  $394 \pm 3$   $\mu$ s, or  $10.9 \pm 0.1$   $\mu$ s per spatial location per step.

Future directions of our research include hybrid approaches using NG-RCs that combine model-generated and experimentally observed data such as those explored using a traditional RC.<sup>9-12</sup> Also, our method should generalize to two- and three-dimensional fluid dynamics problems where an even greater reduction in the required data set size is anticipated. Combined with our approach of one-step-ahead prediction, a coarser spatiotemporal grid can be used, offering the possibility of greatly speeding up spatiotemporal simulations.

## ACKNOWLEDGMENTS

We gratefully acknowledge discussions of this work with E. Bollt and the financial support of the Air Force Office of Scientific Research, Contract #FA9550-20-1-0177.

## DATA AVAILABILITY STATEMENT

The data that support the findings of this study are available from the corresponding author upon reasonable request.

## Appendix A: Ridge regression Parameter Optimization

We train our model using a supervised learning algorithm where the input data  $\mathbf{x}$  and the desired output  $\mathbf{y}$  are known in advance for the entire training period. Here,  $\mathbf{y}$  is evaluated at time  $t_{m+1}$ , whereas  $\mathbf{x}$  is evaluated at time  $t_m$  because we are making a next-step-ahead prediction. We use Ridge regression to find the matrix of weights  $\mathbf{W}$  that minimizes

$$\|\bar{\mathbf{y}} - \mathbf{y}\|^2 + \alpha \|\mathbf{W}\|^2, \quad (\text{A1})$$

where  $\bar{\mathbf{y}} = \mathbf{W}\mathcal{O}_{total}$  is the model output,  $\mathcal{O}_{total}$  is the feature vector obtained from the input data  $\mathbf{x}$  and  $\alpha$  is the Ridge parameter. Here,  $\|\cdot\|$  represents the L2-norm. When  $\alpha$  is zero, Ridge regression reduces to regular least-square regression. The Ridge parameter adds a penalty term to prevent overfitting.

We use a grid-search procedure to find the optimal  $\alpha$  that maximizes the mean prediction horizon for each case shown in previous sections. Figure 9 shows the optimization results for the cases shown in Fig. 4. For each  $\alpha$ , we calculate the mean prediction horizon for 10 different training sets. For each training set we perform predictions for 10 different initial conditions, totaling 100 predictions per  $\alpha$ . We repeat this process for different training times  $t_{train}$ . Figure 9a shows the optimization for the case where the  $L$  parallel NG-RCs are trained individually with data from the respective spatial region, thus resulting in  $L$  independent  $\mathbf{W}_l$ 's. Figure 9b shows the optimization for the single  $\mathbf{W}$ , where a single NG-RC is trained with concatenated data from all spatial regions so that the ML model respects the translational symmetry. It is seen that the algorithm is not sensitive to the value of  $\alpha$  when  $t_{train} \geq 40$  MTU.

## Appendix B: Computational Complexity

Here, we provide an estimation of the computational complexity our parallel NG-RC approach in comparison to the other RC-based approaches mentioned above. The main contribution to the computational complexity for both the NG-RC and the regular RC is performing the Ridge regression, which scales as  $\mathcal{O}(Md_{total}^2)$  for  $M$  training points and  $d_{total}$  features. The comparison for the extended Lorenz96 system

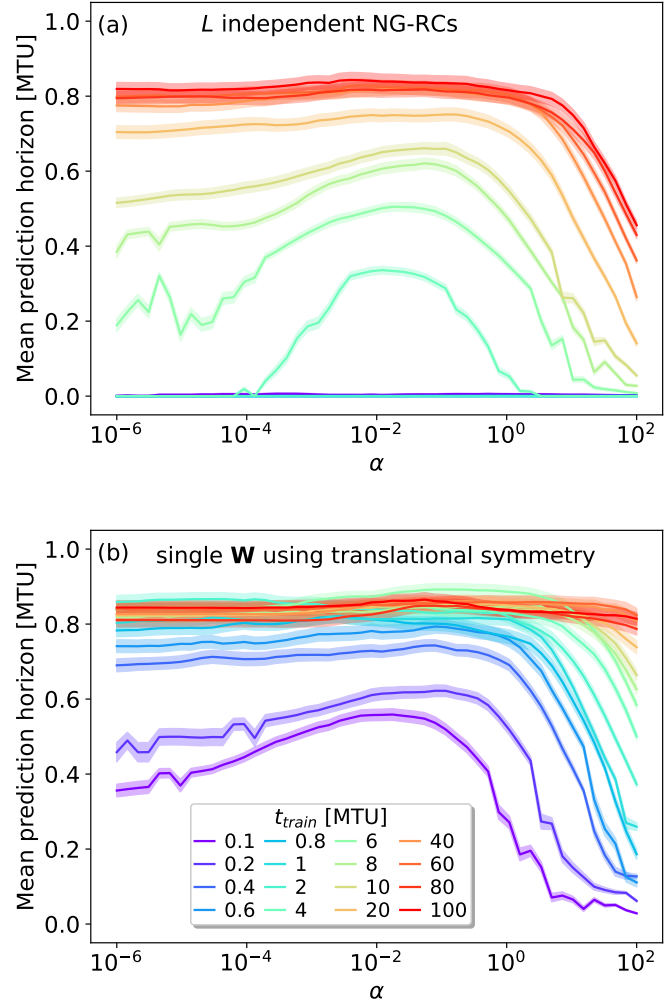


FIG. 9. Ridge parameter optimization for the results shown in Fig. 4. Mean prediction horizon as function of the Ridge parameter  $\alpha$  for different training times (see legend color code) for the case of (a)  $L$  independent NG-RCs and (b) single  $\mathbf{W}$  using translational symmetry. The colored area around the curves represent the standard deviation of the mean.

with  $L = J = I = 8$  and  $L = 40, J = I = 0$  are shown in Tables I and II, respectively. Note that, for the case where we train a single  $\mathbf{W}$  respecting the translational symmetry (first row of each table), the number of training points is multiplied by the number of spatial locations  $L$  to reflect the training data concatenation as discussed in previous sections.

In our analysis for the RC complexity, we do not account for the cost of multiplying the nodes states with the adjacency matrix that represent the network because these RC approaches use neural networks with sparse connectivity (we assume this fact when it is not stated). Also, we do not take into account special function evaluation costs, such as the hyperbolic tangent present in the traditional RC. For the NG-RC, we do not take into account the computational cost of the feature vector creation that happens before training.

	ML model	M	$d_{total}$	$N_{in}$	$N_{out}$	Parallel units trained	Speed up
Our approach - Respecting symmetry	NG-RC	$400 \times 8$	136	5	1	-	-
Our approach - $L$ independent NG-RCs	NG-RC	4,000	136	5	1	8	10
Chattopadhyay <i>et al.</i> <sup>6</sup>	RC	500,000	5,000	8	8	-	$2.1 \times 10^5$
Pyle <i>et al.</i> <sup>7</sup>	NG-RC	500,000	495	8	8	-	$2.1 \times 10^3$

TABLE I. Training complexity comparison of different ML approaches for prediction of the extend Lorenz96 system with  $L = J = I = 8$ .

	ML model	M	$d_{total}$	$N_{in}$	$N_{out}$	Parallel units trained	Speed up
Our approach - Respecting symmetry	NG-RC	$100 \times 40$	136	5	1	-	-
Our approach - $L$ independent NG-RCs	NG-RC	6,000	136	5	1	40	60
Vlachas <i>et al.</i> <sup>14</sup>	RC	100,000	3,000	10	2	20	$2.4 \times 10^5$
Platt <i>et al.</i> <sup>32</sup>	RC	40,000	720	6	2	20	$5.6 \times 10^3$

TABLE II. Training complexity comparison of different ML approaches for prediction of the extend Lorenz96 system with  $L = 40$  and  $J = I = 0$ .

- <sup>1</sup>A. Winfree, *When Time Breaks Down* (Princeton University Press, 1987).
- <sup>2</sup>L. Illing, D. J. Gauthier, and R. Roy, *Controlling Optical Chaos, Spatio-Temporal Dynamics, and Patterns*, edited by P. Berman, C. Lin, and E. Arimondo, Advances In Atomic, Molecular, and Optical Physics, Vol. 54 (Academic Press, 2007) pp. 615–697.
- <sup>3</sup>P. Holmes, J. L. Lumley, and G. Berkooz, *Turbulence, Coherent Structures, Dynamical Systems and Symmetry*, Cambridge Monographs on Mechanics (Cambridge University Press, 1996).
- <sup>4</sup>E. Lorenz, “Predictability: a problem partly solved,” in *Proc. Seminar on Predictability*, Vol. 1 (ECMWF, Reading, Berkshire, United Kingdom, 1996) pp. 1–18.
- <sup>5</sup>D. S. Wilks, “Effects of stochastic parametrizations in the Lorenz ’96 system,” *Q. J. R. Meteorol. Soc.* **131**, 389–407 (2005).
- <sup>6</sup>A. Chattopadhyay, P. Hassanzadeh, and D. Subramanian, “Data-driven predictions of a multiscale Lorenz 96 chaotic system using machine-learning methods: reservoir computing, artificial neural network, and long short-term memory network,” *Nonlinear Process. Geophys.* **27**, 373–389 (2020).
- <sup>7</sup>R. Pyle, N. Jovanovic, D. Subramanian, K. V. Palem, and A. B. Patel, “Domain-driven models yield better predictions at lower cost than reservoir computers in Lorenz systems,” *Philos. Trans. R. Soc. A Math. Phys. Eng. Sci.* **379**, 20200246 (2021).
- <sup>8</sup>H. D. I. Abarbanel, P. J. Rozdeba, and S. Shirman, “Machine Learning: Deepest Learning as Statistical Data Assimilation Problems,” *Neural Comput.* **30**, 2025–2055 (2018).
- <sup>9</sup>A. Wikner, J. Pathak, B. Hunt, M. Girvan, T. Arcomano, I. Szunyogh, A. Pomerance, and E. Ott, “Combining machine learning with knowledge-based modeling for scalable forecasting and subgrid-scale closure of large, complex, spatiotemporal systems,” *Chaos* **30**, 053111 (2020).
- <sup>10</sup>H. Fan, J. Jiang, C. Zhang, X. Wang, and Y.-C. Lai, “Long-term prediction of chaotic systems with machine learning,” *Phys. Rev. Research* **2**, 012080(R) (2020).
- <sup>11</sup>A. Wikner, J. Pathak, B. R. Hunt, I. Szunyogh, M. Girvan, and E. Ott, “Using data assimilation to train a hybrid forecast system that combines machine-learning and knowledge-based components,” *Chaos* **31**, 053114 (2021).
- <sup>12</sup>T. Arcomano, I. Szunyogh, A. Wikner, J. Pathak, B. R. Hunt, and E. Ott, “A hybrid approach to atmospheric modeling that combines machine learning with a physics-based numerical model,” *Journal of Advances in Modeling Earth Systems* **14**, e2021MS002712 (2022).
- <sup>13</sup>A. Chattopadhyay, M. Mustafa, P. Hassanzadeh, E. Bach, and K. Kashinath, “Towards physics-inspired data-driven weather forecasting: integrating data assimilation with a deep spatial-transformer-based u-net in a case study with era5,” *Geoscientific Model Development* **15**, 2221–2237 (2022).
- <sup>14</sup>P. Vlachas, J. Pathak, B. Hunt, T. Sapsis, M. Girvan, E. Ott, and P. Koumoutsakos, “Backpropagation algorithms and reservoir computing in recurrent neural networks for the forecasting of complex spatiotemporal dynamics,” *Neural Netw.* **126**, 191–217 (2020).
- <sup>15</sup>U. Parlitz and C. Merkwirth, “Prediction of spatiotemporal time series based on reconstructed local states,” *Phys. Rev. Lett.* **84**, 1890–1893 (2000).
- <sup>16</sup>S. Ørstavik and J. Stark, “Reconstruction and cross-prediction in coupled map lattices using spatio-temporal embedding techniques,” *Physics Letters A* **247**, 145–160 (1998).
- <sup>17</sup>D. J. Gauthier, E. Bollt, A. Griffith, and W. A. S. Barbosa, “Next generation reservoir computing,” *Nat. Commun.* **12**, 5564 (2021).
- <sup>18</sup>Y.-C. Lai, “Finding nonlinear system equations and complex network structures from data: A sparse optimization approach,” *Chaos* **31**, 082101 (2021).
- <sup>19</sup>E. Bollt, “On explaining the surprising success of reservoir computing forecaster of chaos? the universal machine learning dynamical system with contrast to var and dmd,” *Chaos* **31**, 013108 (2021).
- <sup>20</sup>J. Pathak, A. Wikner, R. Fussell, S. Chandra, B. R. Hunt, M. Girvan, and E. Ott, “Hybrid forecasting of chaotic processes: Using machine learning in conjunction with a knowledge-based model,” *Chaos* **28**, 041101 (2018).
- <sup>21</sup>J. Pathak, B. Hunt, M. Girvan, Z. Lu, and E. Ott, “Model-free prediction of large spatiotemporally chaotic systems from data: A reservoir computing approach,” *Phys. Rev. Lett.* **120**, 024102 (2018).
- <sup>22</sup>Z. Lu, J. Pathak, B. Hunt, M. Girvan, R. Brockett, and E. Ott, “Reservoir observers: Model-free inference of unmeasured variables in chaotic systems,” *Chaos* **27**, 041102 (2017).
- <sup>23</sup>J. Herteux and C. R ath, “Breaking symmetries of the reservoir equations in echo state networks,” *Chaos* **30**, 123142 (2020).
- <sup>24</sup>W. A. S. Barbosa, A. Griffith, G. E. Rowlands, L. C. G. Govia, G. J. Ribeill, M.-H. Nguyen, T. A. Ohki, and D. J. Gauthier, “Symmetry-aware reservoir computing,” *Phys. Rev. E* **104**, 045307 (2021).
- <sup>25</sup>M. Favoni, A. Ipp, D. I. M uller, and D. Schuh, “Lattice gauge equivariant convolutional neural networks,” *Phys. Rev. Lett.* **128**, 032003 (2022).
- <sup>26</sup>M. Oberlack, S. Hoyas, S. V. Kraheberger, F. Alc antara- vila, and J. Laux, “Turbulence statistics of arbitrary moments of wall-bounded shear flows: A symmetry approach,” *Phys. Rev. Lett.* **128**, 024502 (2022).
- <sup>27</sup>Z. Liu and M. Tegmark, “Machine learning hidden symmetries,” *Phys. Rev. Lett.* **128**, 180201 (2022).
- <sup>28</sup>E. N. Lorenz, “Designing chaotic models,” *J. Atmos. Sci.* **62**, 1574–1587 (2005).
- <sup>29</sup>T. Thornes, P. D uben, and T. Palmer, “On the use of scale-dependent precision in earth system modelling,” *Q. J. R. Meteorol. Soc.* **143**, 897–908 (2017).
- <sup>30</sup>A. Chattopadhyay, A. Subel, and P. Hassanzadeh, “Data-driven superparameterization using deep learning: Experimentation with multiscale Lorenz 96 systems and transfer learning,” *J. Adv. Model. Earth Syst.* **12**, e2020MS002084 (2020).
- <sup>31</sup>Mirko Goldmann, Claudio R. Mirasso, Ingo Fischer and Miguel C. Soriano, private communication.
- <sup>32</sup>J. A. Platt, S. G. Penny, T. A. Smith, T.-C. Chen, and H. D. I. Abarbanel, [arXiv:2201.08910](https://arxiv.org/abs/2201.08910).